# Texture Evolution during Isothermal, Isostrain and Isobaric Loading of Polycrystalline Shape Memory NiTi

**D. E. Nicholson[1, †], S. A. Padula II[2], O. Benafan[2] and R. Vaidyanathan[1,a)]**

[1]Advanced Materials Processing and Analysis Center (AMPAC); Materials Science and Engineering Department; Mechanical and Aerospace Engineering Department; University of Central Florida, 12760 Pegasus Drive, Orlando, FL 32816, USA

[†]Presently at, The Boeing Company, 6300 James S. McDonnell Blvd., Berkeley, MO 63134, USA

[2]NASA Glenn Research Center, 21000 Brookpark Road, Cleveland, OH 44135, USA

*In situ* neutron diffraction was used to provide insight into martensite variant microstructures during isothermal, isobaric, and isostrain loading in shape memory NiTi. Results show variant microstructures were equivalent for the corresponding strain and more importantly, the reversibility and equivalency was immediately evident in variant microstructures that were first formed isobarically but then reoriented to a near random self-accommodated microstructure following isothermal deformation. Variant microstructures formed isothermally were not significantly affected by a subsequent thermal cycle under constant strain. In all loading cases considered, the resulting variant microstructure correlated with strain and did not correlate with stress. Based on the ability to select a variant microstructure for a given strain despite thermomechanical loading history, the results demonstrated here can be obtained by following any sequence of thermomechanical loading paths over multiple cycles. Thus for training shape memory alloys (repeating thermomechanical cycling to obtain the desired variant microstructure), optimal paths can be selected so as to minimize the number of training cycles required thereby increasing the overall stability and fatigue life of these alloys in actuator or medical applications.

[a)]Electronic mail: raj@ucf.edu.

Shape memory alloys (SMAs) have the ability to recovery their pre-deformed shape against external loads thus enabling work output in actuator applications. However, the full-scale commercialization of SMA enabled actuator technologies has been limited in the absence of a comprehensive understanding of these alloys under general loading conditions and associated deformation processes (primarily due to a limited understanding of the evolutionary response). With recoverable strains exceeding 4%, near equiatomic NiTi has been the most extensively used alloy for SMA actuator technologies thus far. The recovery process occurs by way of a reversible thermoelastic martensitic phase transformation from a monoclinic (B19') martensite phase to a cubic (B2) austenite phase.[1,2] Previously, *in situ* neutron diffraction has been used to correlate macroscopic behavior with the associated deformation mechanism in polycrystalline shape memory NiTi.[3-9] A majority of these experiments have mainly examined either isothermal[3-7] (deformation at constant temperature) or isobaric[6-9] (thermal cycling to temperatures above and below the phase transformation temperatures under constant stress) loading while none build connections between the two loading paths. Furthermore, experiments examining isostrain (thermal cycling to temperatures above and below the phase transformation temperatures under constant strain) loading have been limited[10,11] and could further our understanding of the use of SMAs in applications, e.g., reinforced composites, couplings, etc.

The objective of this work is thus to provide unique micromechanical and microstructural insight into the isothermal, isobaric, and isostrain loading of SMA with emphasis on providing connections in terms of the texture between these loading paths. This is accomplished by recourse to subjecting a polycrystalline shape memory NiTi SMA to *in situ* neutron diffraction wherein information representative of the bulk is determined in carefully selected experiments involving combined loading sequences. The results are analyzed and presented in the context of

the reversible thermoelastic nature of the martensitic transformation in SMAs and its implications for the durability of these alloys.

The material used was a binary NiTi alloy (nominal composition 49.9 at.% Ni), produced by Special Metals (now SAES Smart Materials, New Hartford, NY). Ten-millimeter rods were produced in the hot-rolled/hot-drawn and hot-straightened condition. Cylindrical dog-bone samples were machined to a 5.08 mm gauge diameter with threaded ends. The stress free phase transformation temperatures; martensite finish ($M_f$), martensite start ($M_s$), austenite start ($A_s$) and austenite finish ($A_f$) were previously[8] determined by differential scanning calorimetry to be 46, 71, 86 and 109±2°C, respectively.

All experiments were performed *in situ* in "time-of-flight" mode using the Spectrometer for Materials Research at Temperature and Stress (SMARTS)[12] at Los Alamos National Laboratory or the VULCAN[13] engineering diffractometer at Oak Ridge National Laboratory. At both SMARTS and VULCAN the loading axis forms a 45° angle with the incident neutron beam. Two detector banks are positioned at opposing 90° angles relative to the beam which allows for reflections from lattices planes perpendicular and parallel to the loading axis to be captured. Results presented henceforth will correspond to reflections from lattices planes perpendicular to the loading axis unless otherwise stated. Macroscopic measurements were made by extensometry (10 mm gauge length and strain resolution of $5 \times 10^{-5}$).

Two stress-free thermal cycles (i.e., isobaric loading at 0 MPa) between room temperature (RT) and 200 °C were performed prior to every experiment after the specimen was installed in the load frame. This was done to relieve any residual stresses produced by processing, machining or installation of the sample and to establish initially, a self-accommodated B19′ martensite microstructure. All isothermal loading was performed in strain

control (at a strain rate of $10^{-4}$) at SMARTS and displacement control (manually, while strain was monitored by extensometry) at VULCAN. It is implicit that prior to an isostrain or isobaric loading cycle the specimen was isothermally loaded (below the $M_f$ temperature) to that strain or stress, respectively. A total of three experiments were performed as follows. Two experiments performed at SMARTS include: one compression-tension (i.e., compression followed by tension) isothermal loading cycle to ±4% strain, then back to 0% strain at RT; and one isostrain loading cycle at 2% tensile strain between 40 °C and 165 °C. Isobaric and isothermal loading was performed at VULCAN in one experiment in the following order: one isobaric loading cycle at 100 MPa tension between RT and 165 °C; compressive isothermal loading to -1.0% strain; two isobaric loading cycles at 0 MPa between RT and 165 °C; and isothermal loading to 3.9% tension at RT. Neutron diffraction spectra were acquired at select points throughout all experiments as shown in context of the results. To ensure adequate statistics for analyses a hold time of 30 min and 15 min at SMARTS and VULCAN, respectively, was used to acquire each spectrum. Neutron diffraction spectra were analyzed using Rietveld refinement implemented by General Structure Analysis System (GSAS).[14] Inverse pole figures (IPFs), which represent the distribution of a selected direction in the specimen relative to the crystal axes in multiples of random distribution (implicit in the following discussion with 1 corresponding to random distribution), were generated from the refinements as previously outlined[15] and plotted with generic mapping tools.[16]

A random self-accommodated martensite variant microstructure was established as indicated by a maximum intensity of 1.78 (within ±0.2 of previous work on this alloy[3]) in the IPF at the initial condition (0 MPa stress and 0% strain) in Figure 1. Figure 1 shows the macroscopic response of NiTi under isothermal compressive loading to -4% strain, followed by

tensile loading to 4% strain and finally compressive loading to 0% strain (from extensometry, as shown by the solid black line). The first segment (0 to -4% strain) of isothermal compressive loading has been well studied and split into multiple loading regimes with corresponding deformation mechanisms by recourse to correlation of IPFs with macroscopic deformation[5,6,8], e.g., in this case elastic deformation (up to 200 MPa) and detwinning and variant conversion (occurring at stresses as low as 50 MPa). At a maximum compressive strain of -4% the specimen was within the end of the region in which detwinning and variant conversion was the dominant deformation mechanism although others, e.g., slip and dislocation based plasticity, may be active to a limited degree. Direct evidence of the selection of martensite variants by variant reorientation and detwinning was observed as an increase in intensity at the 111 pole in the corresponding IPF. A maximum intensity (near the 111 pole) of 3.00 was observed and was comparable to a maximum intensity (at the same location) of 2.96 as observed in Ref. [3] at -3.7% strain. The variants that were selected in compression reoriented to a near random self-accommodated orientation when the deformation was reversed (from -4% to 0% strain) and the macroscopic strain approaches zero, thus demonstrating the reversibility of variant reorientation and detwinning processes (observed macroscopically by the onset and continuation of the detwinning and variant reorientation stress-strain plateau). Following this first load reversal at 0% strain, remnant or residual texture was observed as an increase in intensity at the 111 pole and reappearance of the 010 pole with an increase in maximum intensity (near the 010 pole) from 1.78 to 1.93 when compared to the initial IPF. This aforementioned texture evolution could also have contributions from detwinning given the magnitude of the stresses.

When deformation was continued in tension to 4% strain, the preferred selection of corresponding martensite variants was observed as an increase in intensity at the -150 pole in the

IPF. A maximum intensity (near the -150 pole) of 5.18 was observed and was comparable to a maximum intensity (near the same location) of 6.49 in Ref. [3] in which the specimen was loaded directly to 5.3% strain. These variants reoriented to a near random self-accommodated orientation when the deformation was reversed and the macroscopic strain approaches zero, again demonstrating the reversibility. The amount of remnant or residual texture increased at the 010 pole when compared to the IPF at 0% strain following the first load reversal as indicated by an increase in the maximum intensity (near the 010 pole) from 1.76 to 2.30 when compared to the initial IPF. Overall, similar texture was observed at zero strain despite a significant difference in stress following the initial, first and second deformation cycles (0 MPa, 330 MPa and -234 MPa, respectively). In all cases of such isothermal loading (i.e., compression followed by tension and solely[3] compression or tension), the resulting variant microstructure correlated with the macroscopic uniaxial strain and did not correlate with the compressive or tensile state of stress. In addition to detwinning, the residual texture observed at zero strain may be the result of some variants pinned by dislocations which accumulated during the isothermal reverse loading process and/or slip. The accumulation of dislocations at both junction plane areas and within martensite twins have been observed by transmission electron microscopy in similar reverse loading experiments.[17] By recourse to IPFs, indirect evidence of slip has previously been captured as the slight rotation of the -150 to 010 poles during tensile deformation.[6] Recent progress has been made towards quantifying the contributions of each these deformation mechanisms (i.e., elastic, detwinning/variant reorientation, deformation twinning and slip) to the overall strain using a micromechanical model based diffraction data analysis framework which shows all such mechanisms to be active to a limited degree within the limits studied here.[5,18]

Figure 2 shows the macroscopic response for one thermal cycle to temperatures above and below the phase transformation under a constant tensile strain (isostrain loading) of 2%. The starting IPF (not shown) at 0 MPa stress and 0% strain at RT with a maximum intensity of 1.91 was comparable to the starting IPF in Figure 1, corresponding to a self-accommodated starting B19′ martensite microstructure. The specimen was isothermally loaded in strain control to 2% strain (Points A to B) and the variants preferentially selected in tension were consistent with the results seen in Figure 1 (from the IPF corresponding to Point B at a stress of 262 MPa). This strain was held constant in strain control, followed by the specimen being thermally cycled from 40 °C to 165 °C (Points B to C) and a resulting blocking stress (maximum of 450 MPa) was observed as a result of the phase transformation to the austenite phase at Point C. Note, no significant texture changes were observed in the austenite phase. When the specimen was cooled to 40 °C (Point C to D) through the phase transformation, the stress relaxed to 6 MPa. The IPF corresponding to Point D showed a similar variant microstructure to that of Point B with a small decrease in the maximum intensity from 3.57 to 3.20 near the -150 pole. Deformation processes associated with shape setting[10] (e.g., plastic deformation and recovery processes) may be active to a limited degree and may have contributed to the relaxation of stress and the slight decrease in texture. Overall, the macroscopic stress from the isothermal strain relaxed to near zero with no concomitant change in the variant microstructure following the first thermal cycle, establishing the correspondence between the resulting variant microstructure and the macroscopic strain during isostrain loading despite the temperature excursion.

Figure 3 shows IPFs corresponding to isothermal (indicated by solid arrows) and isobaric (indicated by dashed arrows) loading in the same experiment. The starting IPF (Point I) at 0 MPa stress and 0% strain at RT with a maximum intensity of 1.87 was comparable to the starting IPF

in Figure 1. This is indicative of a self-accommodated martensite phase and establishes a basis for comparisons between the IPFs generated from experiments at SMARTS (i.e., Figs. 1 and 2) and VULCAN (i.e., Fig. 3). The corresponding macroscopic state in Roman numerals is given above each IPF in Fig. 3 and corresponds to those shown in Figs. 1 and 4. Initial isothermal loading at RT from 0 to 100 MPa (Point I to II) was dominated by elastic deformation with limited detwinning and/or variant reorientation, as indicated by no significant change in the maximum intensity observed in the IPFs and was consistent with Refs. [2,5,9]. The specimen was held constant at a tensile stress of 100 MPa and thermally cycled between RT and 165 °C (i.e., isobaric loading from Point II to III) resulting in a tensile strain of 3.9 % (often referred to as transformation strain) at Point III, as shown by the dashed line in Fig. 4. The variant microstructure resulted in a maximum intensity of 5.83 near the -150 pole which compared well with the variant microstructure selected in tension at the equivalent strain generated by isothermal deformation in Fig. 1 and Ref. [2].

From 3.9% strain (Point III), the specimen was isothermally deformed in compression at RT to -1.0% strain (Point VI), as shown by the dashed line in Fig. 1. Variant reorientation and detwinning was observed macroscopically in Fig. 1 as the onset (Point IV) and continuation of the stress-strain plateau (Points IV through VI). The corresponding IPFs show that variants preferentially selected during tensile isobaric loading reoriented to a near random self-accommodated orientation with some residual texture during isothermal loading from Points III to VI. This behavior was consistent with deformation following the second load reversal (4% to 0% strain) in Fig. 1. From Point VI, the specimen was unloaded to 0 MPa resulting in -0.6% strain and a maximum intensity of 2.65 in the corresponding IPF at Point VII. This was followed by two isobaric cycles at 0 MPa performed between 30 °C and 165 °C which resulted in a self-

accommodated variant microstructure with some residual texture at 0.5% strain (macroscopically corresponding to the solid line in Fig.4). At Point VIII, the specimen both macroscopically and microstructurally resembled the starting state (Point I) with the exception of some residual texture. The specimen was then isothermally loaded in tension to 3.9% at RT (macroscopically corresponding to Points VIII to IX in Fig. 1) and variants were preferentially selected as indicated by a maximum intensity of 5.32 near the -150 pole. This variant microstructure was equivalent to that observed during isobaric loading (Points II to III in Fig. 3) and isothermal loading in Fig. 1 and Ref. [2].

Overall, the variant microstructures were equivalent for the corresponding strain and more importantly, the reversibility and equivalency were immediately evident in a variant microstructure that was first formed isobarically but then reoriented to a near random self-accommodated structure following isothermal deformation. In all cases of such loading (tensile or compressive isothermal, isobaric or isostrain), the resulting B19′ martensite variant microstructure correlated with the macroscopic uniaxial strain and did not correlate with the state of stress. Based on the ability to select a particular variant microstructure for a given strain despite loading history (e.g., the second load reversal following the first load reversal in Fig. 1 or Points VIII to IX following Points I through VIII in Fig. 3), the results demonstrated in this letter can be obtained by following any sequence of thermomechanical loading paths over multiple cycles with the exception of residual texture (the formation of which saturates with cycling[19]). Thus for training SMAs (repeating thermomechanical cycling to obtain the desired variant microstructure), optimal paths can be selected so as to minimize the number of training cycles required thereby increasing the overall stability and fatigue life of SMAs. The foundation for this observed behavior lies in the fundamental reversibility of detwinning and variant

reorientation processes in B19′ martensite and the phase transformation between B19′ martensite and B2 austenite. These reversible deformation mechanisms dominate over the irreversible deformation mechanisms (within the limits investigated), the effects of which are minimized by the accommodative nature of B19′ martensite as observed in the remnant or residual texture.

D.E.N. and R.V. acknowledge funding from the NASA Fundamental Aeronautics Program., Supersonics Project (Grant No. NNX08AB51A), Subsonic Fixed Wing Project (Grant No. NNX11AI57A), and most recently the Aeronautical Sciences Project. The authors thank T. Sisneros, B. Clausen, and D.W. Brown at LANL and H.D. Skorpenske and K. An at ORNL for technical support. The authors also thank S. Qiu (formerly at UCF) for helpful discussions. This work has benefited from the use of the Lujan Neutron Scattering Center at LANSCE, which is funded by the Office of Basic Energy Sciences (DOE). LANL is operated by Los Alamos National Security LLC under DOE under Contract No. DE-AC52-06NA25396. The work has also benefited from the use Spallation Neutron Source at ORNL, which is funded by the Division of Scientific User Facilities, Office of Basic Energy Sciences, US Department of Energy under Contract DE-AC05-00OR22725 with UT-Battelle, LLC.

[1] K. Otsuka and C. M. Wayman, *Shape Memory Materials*, (Cambridge University Press, Cambridge, 1999).

[2] K. Bhattacharya, *Microstructure of Martensite: Why It Forms and How It Gives Rise to the Shape-Memory Effect?* (Oxford University Press, New York, 2003).

[3] S. Qiu, B. Clausen, S. A. Padula II, R. D. Noebe, and R. Vaidyanathan, Acta Mater. **59** (13), 5055 (2011).

[4] O. Benafan, R. D. Noebe, S. A. Padula II, A. Garg, B. Clausen, S. Vogel, and R. Vaidyanathan, International Journal of Plasticity **51**, 103 (2013).

[5] A. P. Stebner, D. W. Brown, and L. C. Brinson, Acta Mater. **61** (6), 1944 (2013).

[6] O. Benafan, S. A. Padula II, R. D. Noebe, T. Sisneros, and R. Vaidyanathan, Journal of Applied Physics **112**, 093510 (2012).

[7] O. Benafan, R. D. Noebe, S. A. Padula II, D. J. Gaydosh, B. A. Lerch, A. Garg, G. S. Bigelow, K. An, and R. Vaidyanathan, Scripta Materialia **68**, 571 (2013).

[8] S. Qiu, V. B. Krishnan, S. A. Padula, R. D. Noebe, D. W. Brown, B. Clausen, and R. Vaidyanathan, Applied Physics Letters **95** (14), 141906 (2009).

[9] B. Ye, B. S. Majumdar, and I. Dutta, Applied Physics Letters **91** (6), 061918 (2007).

[10] O. Benafan, S. A. Padula II, R. D. Noebe, D. W. Brown, B. Clausen, and R. Vaidyanathan, Acta Materialia **61** (10), 3585 (2013).
[11] O Benafan, RD Noebe, TJ Halsmer, SA Padula II, GS Bigelow, DJ Gaydosh, and A Garg, Shape Memory and Superelasticity, 1 (2016).
[12] M. A. M. Bourke, D. C. Dunand, and E. Ustundag, Appl. Phys. A **74**, S1707 (2002).
[13] K. An, H. D. Skorpenske, A. D. Stoica, D. Ma, X. Wang, and E. Cakmak, Metallurgical and Materials Transactions A **42** (1), 95 (2011).
[14] A.C. Larson and R. B. Von Dreele, Los Alamos National Laboratory Report LAUR 86-748 (2004).
[15] R. B. Von Dreele, J. Appl. Cryst. **30**, 517 (1997).
[16] P. Wessel and W. H. F. Smith, EOS Trans. Am. Geophys. Union 76, 329 (1995).
[17] Z. L. Xie, Y. Liu, and J. Van Humbeeck, Acta Materialia **46** (6), 1989 (1998).
[18] A. P. Stebner, S. C. Vogel, R. D. Noebe, T. Sisneros, B. Clausen, D. W. Brown, A. Garg, and L. C. Brinson, Journal of the Mechanics and Physics of Solids **61** (11), 2302 (2013).
[19] O. Benafan, R. D. Noebe, S. A. Padula II, D. W. Brown, S. Vogel, and R. Vaidyanathan, International Journal of Plasticity **56**, 99 (2014).

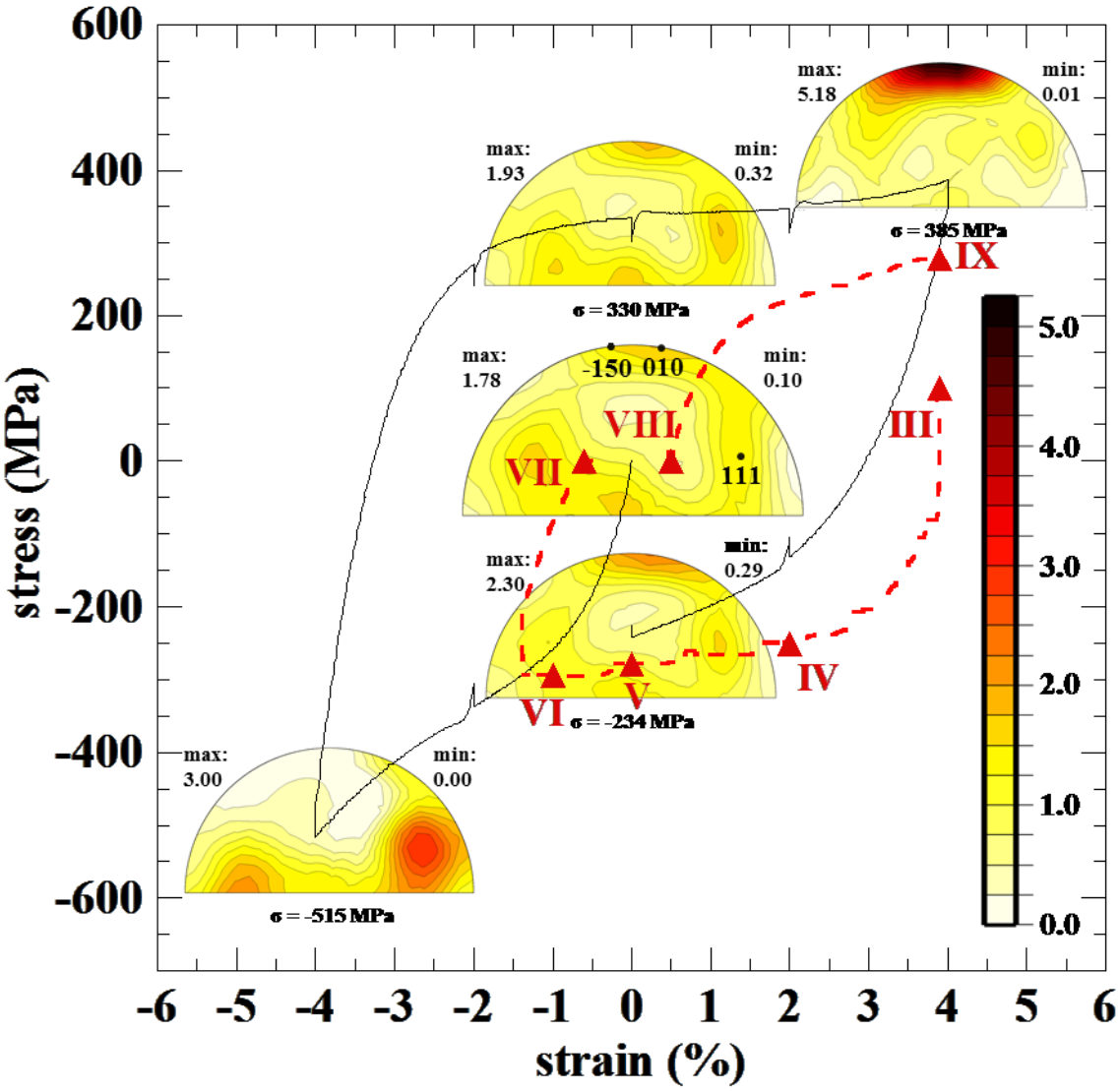


FIG. 1. Inverse pole figures (IPFs) corresponding to the macroscopic response of B19′ martensitic NiTi under isothermal compressive, followed by tensile, and finally compressive reverse loading (solid line). Also shown as a dashed line is the macroscopic isothermal path

corresponding to Points III-IX (indicated by ▲) in FIG. 3. For clarity in presentation, the scale chosen is unique to this figure.

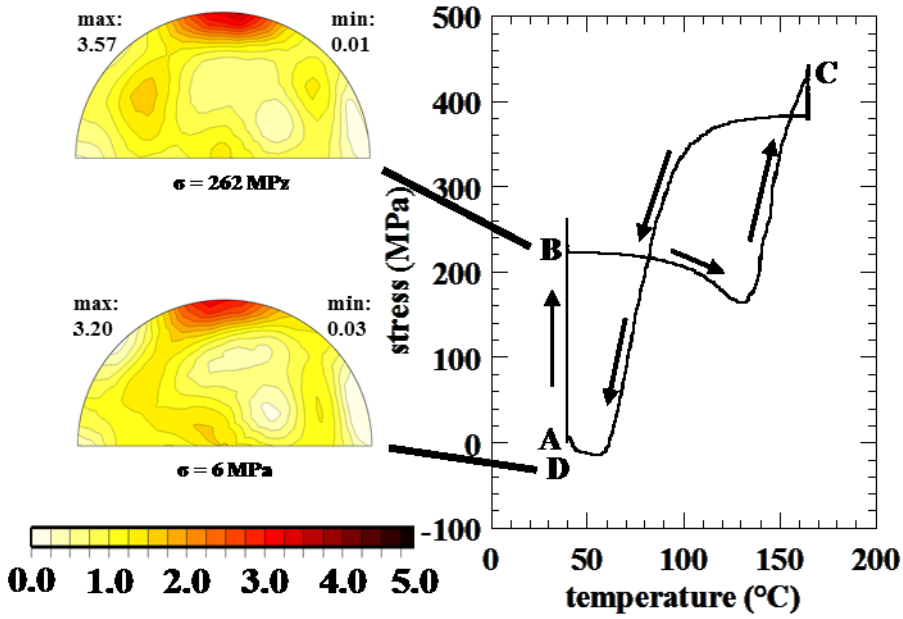


FIG. 2. Inverse pole figures (IPFs) obtained before (Point B) and after (Point D) a thermal cycle above and below the phase transformation temperature at a constant strain of 2% and the corresponding macroscopic stress-temperature response. For clarity in presentation, the scale chosen is unique to this figure.

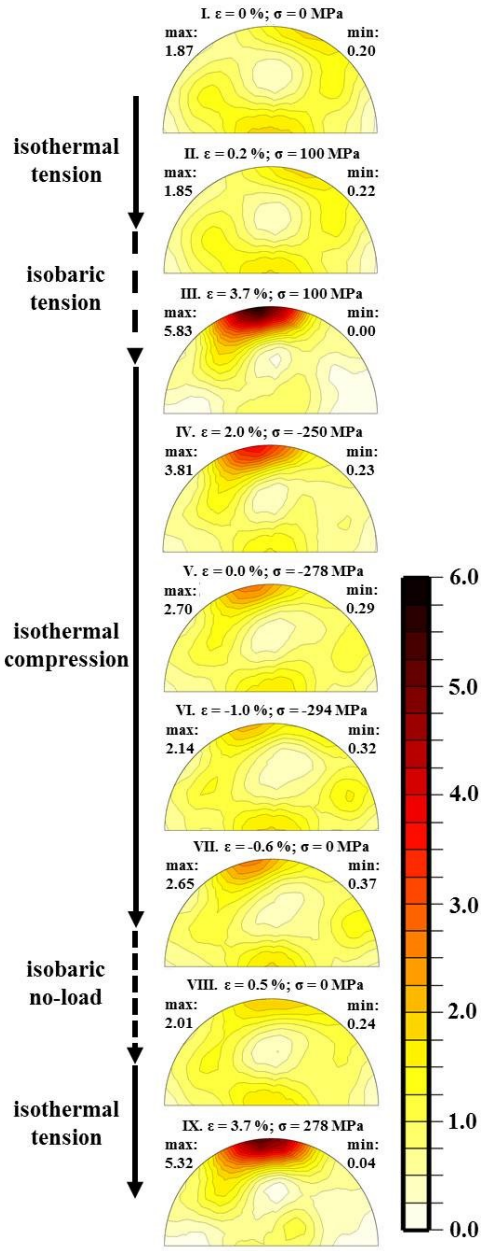


FIG. 3. Inverse pole figures (IPFs) corresponding to mixed isothermal (solid arrows) and isobaric (dashed arrows) loading in the same experiment. During isobaric loading the sample was

thermally cycled above and below the phase transformation temperature, once from Points II to III and twice from Points VII to VIII. The Roman numbering scheme adopted above each IPF is consistent with that shown in FIG 1 and FIG 4. For clarity in presentation, the scale chosen is unique to this figure.

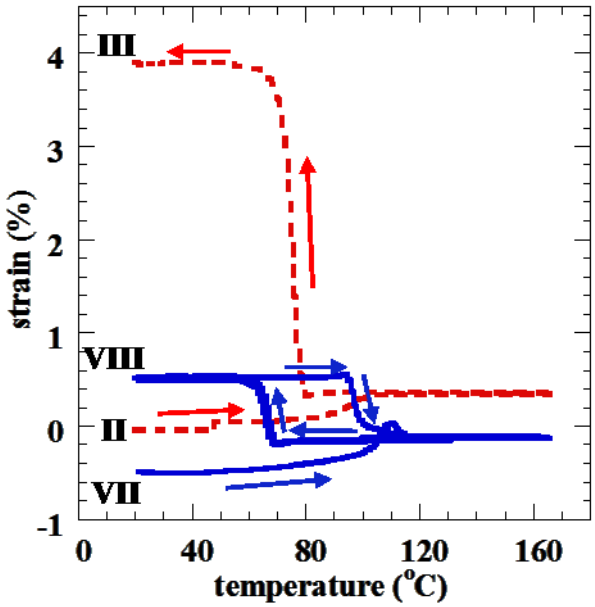


FIG. 4. Macroscopic isobaric paths corresponding to Points II-III (dashed line) and Points VII-VIII (solid line) in FIG. 3.